

# ASSESSMENT OF COMPUTATIONAL TOOLS FOR THE PREDICTION OF BVI NOISE

Sabino Loiodice<sup>1</sup>, Anastasios Kokkalis<sup>1</sup>, Dimitris Drikakis<sup>1</sup>, Guillaume Perez<sup>2</sup>, Giovanni Bernardini<sup>3</sup>, Massimo Gennaretti<sup>3</sup>, Rita Ponza<sup>4</sup>, Michael Hounjet<sup>5</sup>, Harry Brouwer<sup>5</sup>

<sup>1</sup>Department of Aerospace Science, Cranfield University, United Kingdom

<sup>2</sup>Department of Numerical Simulation and Aeroacoustics, ONERA, France

<sup>3</sup>Dipartimento di Ingegneria Meccanica ed Industriale, Roma Tre University, Italy

<sup>4</sup>Aerodynamics Department, Agusta, Italy

<sup>5</sup>National Aerospace Laboratory, NLR, Netherlands

**Key words:** Rotorcraft, FW-H, aeroacoustics, dynamics, aerodynamics, Helishape, Friendcopter.

**Abstract:** The paper presents an assessment of various computational tools pertinent to the prediction of rotor blade induced noise developed by the partners of the Friendcopter project entitled “Integration of Technologies in Support of a Passenger and Environmentally Friendly Helicopter”. The computational tools comprise of coupled aeroelasticity and aerodynamic analysis tools, which provide input to the aeroacoustic codes used for predicting the helicopter footprints and noise levels. As these computational tools will be employed during the design phase of future environmentally friendly helicopters, assessment of their accuracy is required. In the nineties the HELISHAPE consortium embarked into a European research programme on rotorcraft aerodynamics and acoustics conducting a parametric model rotor test. These results have been reported in previous European projects (EROS, ROSAA). The test cases are based on two modern rotors designed by Eurocopter, the EC/ONERA 7A and 7AD, which differ only by their blade tip shape: the 7A has a rectangular blade tip while the 7AD has the SSP8 parabolic tip with taper. The choice of these experimental cases seemed to be the most appropriate ones for assessing the present computational tools. In the paper, we describe the various aeroacoustic methods employed and present a comparative analysis and assessment of the predictive results from these.

## 1 INTRODUCTION

The issue of reducing the noise produced by helicopters is of great interest to the rotorcraft industry and any solutions that contribute to this are very desirable as it would allow helicopters to fly closer to urban regions more hours per day. The current noise regulations imposed by the European Community in 2000 are more stringent than the noise certification requirements created in the 80's (ICAO annex16 chap8, and FAR36 App H). Finally the introduction of noise pollution taxes for some heliports, the obligation to define Land Use Planning prior to any heliport opening have certainly forced the rotorcraft manufacturers to pay more attention to the reduction of noise pollution.

The Friendcopter project is a collaborative European project under the auspices of the EU FP6 research programme. Within this project, are collaborating the most experienced European companies, research institutes and academic institutions in the field of helicopter design. The aim of the project is to obtain environment friendly helicopters, [1], and this will be pursued step by step:

- short term goal: definition of noise abatement flight procedures and cabin and engine noise reduction using noise absorbing structures and active structures control.
- long term goal: lowering of impulsive exterior noise, of excessive cabin vibrations and of high fuel consumption by active blade control.

Definition of noise abatement procedures is the first step to be taken via the use of an optimization suit of software, called HELENA, and produced within the Friendcopter framework, which will rely on experimental and numerical databases. The computational tools presented in this paper will be used primarily to build the numerical database, analyzing various helicopters in different flight conditions. The choice to use both experimental and numerical databases becomes clear once one considers the costs of experiments. Just to give an idea, an acoustic test on a scale model helicopter in a wind tunnel costs around 200k Euro per week without taking into account the design and production costs of the WT model. In flight aeroacoustics experiments are even more expensive.

Numerical predictions represent a valid alternative to experiments once the computational tools used for the analysis are validated and verified against well conducted experiments. The tools presented in this paper have already been validated and verified by the partners, [14][15][19][22], but against different experiments. A key aim of the paper is to assess the prediction codes produced within the Friendcopter framework against the same experiments, so to have an estimation of the differences between the predictions. This will constitute a common base of comparison when the tools will be used to analyze different cases for which experiments won't be available.

Since the main aim of the present study is to compare the computational tools, produced within Friendcopter project, on some cases presenting strong BVI phenomena, the choice from the noise related databases available fell on the wind tunnel experiments conducted in the nineties by the HELISHAPE consortium, [2], in which some of the Friendcopter partners had already cooperated. These experimental results have been already documented in other european projects (EROS, ROSAA), and previously used in literature for validation purposes, [3]-[4]-[5].

The structure of the paper is as follows. First a brief description of rotorcraft noise prediction methodologies is given in section 2. Then the codes utilized in the following calculations are presented in section 3, followed by a brief description of the experimental test case used in section 4. Finally a comparison between the numerical and the experimental results is given and discussed in section 5.

## 2 ROTORCRAFT NOISE

The noise produced by a helicopter rotor is unique and quite different from that produced by any other airborne vehicle. The main sources of rotor generated noise are mainly due to its complex aeromechanics and the unsteady aerodynamic loads acting upon it. Detail examination of the rotor noise generating mechanisms, [13], has made it possible to identify three main components that add together to create this characteristic noise, i.e.:

- I. Blade - Vortex Interaction (BVI) noise due to the interactions between the tip vortex shed from the preceding blade and the following one, Figure 1
- II. High Speed Impulsive (HIS) noise in fast level flight due to the presence of shocks over the blade tip area, and,
- III. Broadband noise.

The focus in this paper is on the prediction of BVI noise and thus the test cases chosen for the comparisons are in the low speed descending flight regime.

Rotorcraft noise prediction methods are based mostly on Lighthill's Acoustic Analogy theory. Lighthill in 1951, [7], affirmed that given a fluctuating fluid flow which occupies only a limited part of a very large volume of fluid at rest, the fluctuations of density of the real fluid are governed by equations similar to the ones occurring in a uniform acoustic medium at rest, but with the presence of a different forcing term, the Lighthill's stress tensor  $T_{ij}$  :

$$\frac{\partial^2}{\partial t^2} \rho' - c_0^2 \nabla^2 \rho' = \frac{\partial^2 T_{ij}}{\partial x_i \partial x_j} \quad (1)$$

In which the quantities with subscript 0 represent the medium at rest,  $\rho'$  is the density fluctuation and:

$$T_{ij} = \rho v_i v_j + (p - p_0) \delta_{ij} - c_0^2 (\rho - \rho_0) \delta_{ij} - e_{ij} \quad (2)$$

with:

$$e_{ij} = \mu \left( \frac{\partial v_i}{\partial x_j} + \frac{\partial v_j}{\partial x_i} - \frac{2}{3} \delta_{ij} \frac{\partial v_k}{\partial x_k} \right) \quad (3)$$

Various approaches have been presented to obtain the integral form of equation ( 1 ). Reminding that the original equation was found in [8] a clear explanation, including an introduction on generalized functions is presented in [10]. Here we will use the approach described from Goldstein, [9], based on Green's Functions. This approach is interesting because it doesn't rely from the start on the free space Green's Function, but imposes this choice in order to arrive at the same conclusion as the one presented by Ffowcs Williams and Hawkins, [8].

Let us start form the inhomogeneous wave equation for a uniformly moving medium for a source distribution  $\gamma$ :

$$\frac{1}{c_0^2} \frac{D_0^2}{D\tau^2} p - \nabla^2 p = \gamma(\bar{y}, \tau) \quad (4)$$

and let  $G(y, \tau | x, t)$  be the solution of:

$$\frac{1}{c_0^2} \frac{D_0^2}{D\tau^2} G - \nabla^2 G = \delta(t - \tau) \delta(\bar{x} - \bar{y}) \quad (5)$$

in a volume  $v(\tau)$  bounded (internally or externally) by a surface  $s(\tau)$  generally moving.  $G$  is called *fundamental solution* of the wave equation.  $G$  is required to satisfy the casualty condition that can be found in [9], where are also shown the passages to obtain the *generalized Green's formula* that relates the value of  $p$  in a generic point  $x$  and time  $t$  with the distribution of sources in the volume  $v(\tau)$ :

$$\int_{-T}^T d\tau \int_{v(\tau)} \gamma(\bar{y}, \tau) G(\bar{y}, \tau | \bar{x}, t) d\bar{y} + \int_{-T}^T d\tau \int_{s(\tau)} \left[ G(\bar{y}, \tau | \bar{x}, t) \left( \frac{\partial}{\partial n} + \frac{\bar{V}'_n}{c_0^2} \frac{D_0}{D\tau} \right) p(\bar{y}, \tau) - p(\bar{y}, \tau) \left( \frac{\partial}{\partial n} + \frac{\bar{V}'_n}{c_0^2} \frac{D_0}{D\tau} \right) G(\bar{y}, \tau | \bar{x}, t) \right] dS(\bar{y}) = \begin{cases} p(\bar{x}, t) & \forall x \subset v(\tau) \\ 0 & \forall x \notin v(\tau) \end{cases} \quad (6)$$

in which:

$$\bar{V}'_n = (\bar{V}_s - \bar{U}) \cdot \hat{n} \quad (7)$$

being  $V_s$  the velocity of the surface  $s(\tau)$  bounding  $v(\tau)$  and  $U$  the velocity of the medium. The equation (6) in case of a stationary medium,  $U=0$ , substituting  $p$  with  $c_0^2 \rho'$  and  $\gamma$  with the second member of (1) becomes:

$$\frac{1}{c_0^2} \int_{-T}^T d\tau \int_{v(\tau)} \frac{\partial^2 T_{ij}}{\partial y_i \partial y_j} G d\bar{y} + \int_{-T}^T d\tau \int_{s(\tau)} \left[ G \left( \frac{\partial}{\partial n} + \frac{\bar{V}'_n}{c_0^2} \frac{\partial}{\partial \tau} \right) \rho' - \rho' \left( \frac{\partial}{\partial n} + \frac{\bar{V}'_n}{c_0^2} \frac{\partial}{\partial \tau} \right) G \right] dS(\bar{y}) = \rho' \quad (8)$$

reminding that:

$$\frac{\partial^2 T_{ij}}{\partial y_i \partial y_j} G - T_{ij} \frac{\partial^2 G}{\partial y_i \partial y_j} = \frac{\partial}{\partial y_i} G \frac{\partial T_{ij}}{\partial y_j} - \frac{\partial}{\partial y_i} T_{ij} \frac{\partial G}{\partial y_j} \quad \text{and} \quad \bar{V}'_n = \bar{V}_s \cdot \hat{n}, \quad \frac{\partial}{\partial n} = n_i \frac{\partial}{\partial y_i}$$

With some manipulations and in presence of solid boundaries:

$$\rho' = \frac{1}{c_0^2} \int_{-T}^T \int_{v(\tau)} \frac{\partial^2 G}{\partial y_i \partial y_j} T_{ij} d\bar{y} d\tau + \frac{1}{c_0^2} \int_{-T}^T \int_{s(\tau)} \frac{\partial G}{\partial y_i} f_i dS(\bar{y}) d\tau + \frac{1}{c_0^2} \int_{-T}^T \int_{s(\tau)} \rho_0 \bar{V}'_n \frac{\partial G}{\partial \tau} dS(\bar{y}) d\tau \quad (9)$$

where:

$$f_i = (p - p_0) n_i + e_{ij} n_j$$

It has to be noted that since now we did not specify at all what kind of function is  $G$  except that it has to satisfy (5) plus the opportune boundary and initial conditions of the problem. If the volume  $v(\tau)$  is unbounded the only choice of  $G$  is the free space Green's Function  $G^0$ :

$$G^0(\bar{y}, \tau | \bar{x}, t) = \frac{1}{4\pi R} \delta\left(\tau - t + \frac{R}{c_0}\right) = \frac{1}{4\pi R} \delta[g(\tau, t, R)] \quad (10)$$

Ffowcs William and Hawkings proposed in their paper, [8], the very successful idea to use the free space Green's function even in presence of bounded domains. Substituting ( 10 ) in the place of G in ( 9 ), we obtain finally, after some passages that can be found in [9] the FW-H equation:

$$\begin{aligned} \rho' = & \frac{1}{4\pi c_0^2} \frac{\partial^2}{\partial x_i \partial x_j} \int_{v(\tau)} \left[ \frac{T_{ij}}{R|1-M_R|} \right]_{\tau=\tau_r^k} d\bar{\eta} - \frac{1}{4\pi c_0^2} \frac{\partial}{\partial x_i} \int_{s(\tau)} \left[ \frac{f_i}{R|1-M_R|} \right]_{\tau=\tau_r^k} dS(\bar{\eta}) \\ & - \frac{1}{4\pi c_0^2} \frac{\partial}{\partial x_i} \int_{v_0} \left[ \frac{\rho_0 \dot{V}_i}{R|1-M_R|} \right]_{\tau=\tau_r^k} d\bar{\eta} + \frac{1}{4\pi c_0^2} \frac{\partial^2}{\partial x_i \partial x_j} \int_{v_0} \left[ \frac{\rho_0 V_i V_j}{R|1-M_R|} \right]_{\tau=\tau_r^k} d\bar{\eta} \end{aligned} \quad (11)$$

The integral equation (11), in terms of density, represents the FW-H equation as presented in [8]. It is possible to rearrange the above equation excluding the first term, known as quadrupole term, that gives a contribution only for transonic and supersonic cases, and transform the space derivatives in time derivatives, using the following property of the delta function:

$$\frac{\partial}{\partial x_i} \left( \frac{\delta(g)}{r} \right) = \frac{\partial}{\partial t} \left( \frac{\delta(g)}{r} \right) \frac{r_i}{r} - \frac{\delta(g)}{r^2} \frac{r_i}{r}$$

It is possible to arrive to the following formulation, in terms of pressure fluctuations  $p'$ , known as Farassat Formulation 1, [10]:

$$p' = \frac{1}{4\pi c_0} \frac{\partial}{\partial t} \int_{s_b} \left[ \frac{\rho_0 c_0 V_n + f_r}{R|1-M_R|} \right]_{\tau=\tau_r^k} dS + \frac{1}{4\pi} \int_{s_b} \left[ \frac{f_i}{R^2|1-M_R|} \right]_{\tau=\tau_r^k} dS \quad (12)$$

or bringing the time derivative in the first term inside the integral using the definition of the retarded time function  $g[t,\tau,R(\tau)]$  that gives:  $\frac{\partial}{\partial t} \Big|_x = \left( \frac{1}{1-M_r} \frac{\partial}{\partial \tau} \Big|_{x_{ret}} \right)$  and applying this transformation to the above equation:

$$\begin{aligned} 4\pi p' = & \int_s \frac{\rho_0 \dot{v}_n}{R|1-M_r|^2} \Big|_{ret} dS + \int_s \frac{\rho_0 v_n \left( R M_r + c_0 M_r - c_0 M^2 \right)}{R^2 |1-M_r|^3} \Big|_{ret} dS \\ & + \frac{1}{c_0} \int_s \frac{\dot{f}_r}{R|1-M_r|^2} \Big|_{ret} dS + \int_s \frac{f_r - f_M}{R^2 |1-M_r|^2} \Big|_{ret} dS + \frac{1}{c_0} \int_s \frac{f_r \left( R M_r + c_0 M_r - c_0 M^2 \right)}{r^2 |1-M_r|^3} \Big|_{ret} dS \end{aligned} \quad (13)$$

and which is know as Farassat Formulation 1A in retarded time.

### 3 COMPUTATIONAL TOOLS

The noise prediction equation ( 11 ) can not be used on its own to predict the noise from a rotor since it only describes the propagation of noise from a source to an observer. The magnitude of the source or sources that contribute to noise generation must be found via aerodynamic prediction tools that if accurate will ensure an accurate aeroacoustic prediction. Furthermore in helicopters' aeroacoustic analysis a stand alone aerodynamic prediction is not

capable to analyze the complex behavior of the vehicle. Even restricting the analysis to the main rotor only, as in the cases presented here, its complex dynamics and aerodynamics, which influence each other, require the use of accurate aeroelasticity predictions.

Hence a prediction chain for rotor noise analysis must model accurately all three main components: the rotor's dynamics, the rotor's aerodynamics and finally the rotor's aeroacoustics. In Table 1 a summary is presented of the characteristics for the five noise prediction computational tools, CT, used for the present calculations.

	CT1	CT2	CT3	CT4	CT5
Dynamics	Y	Y	Y	Y	Same as CT1
Wake geometry computation	Free wake blade : lifting surface Wake : panels	Free wake blade : lifting line Wake : filaments	Free wake	Free wake	Same as CT1
Computation of interaction aerodynamics	Performed by the free wake computation	Performed by a 2D by slices singularity computation			
Aeroacoustics	FW-H	FW-H Source time formulation	FW-H	FW-H	FW-H Advanced time formulation

Table 1: Codes characteristics

The main focus in the present calculations, since the test cases are in low speed descent, is on BVI phenomena, these require an accurate prediction of the rotor wake and of the interaction between this and the blade aerodynamics. In fact as will be clear in the following paragraph all the CT uses a free wake analysis to determine the geometry of the wake. Let us describe now the computational tools employed by the different partners dividing the discussion in the components specified above.

### 3.1 Aeroelasticity and dynamics

As far as the aeroelasticity calculations are concerned, the CT1 code uses an in-house code whose formulation is entirely based on a Finite Element Method (FEM) approach providing modal and frequency response to aerodynamic and inertial loads acting on the blades. This is done via a lifting surface module that determines the aerodynamic load on the deformed blades by means of a free wake vortex lattice formulation. In the current cases the CT1 instead of performing a complete aeroelastic calculation, used as input of the aerodynamic code the detailed rotor kinematics data obtained from the HELISHAPE WT experiments. The CT5 code also uses the aeroelastic calculations performed with CT1.

To determine the blade motion and deformation, CT2 performs an aeroelastic calculation with a beam dynamic model for the blade. To have an accurate evaluation of the aerodynamic loads, the dynamics computation is coupled to the free wake analysis.

The blade structural dynamics for the CT3 is based upon the non linear flap-lag-torsion equations of motion developed by Hodges and Dowell, [17][18]. These are based on a beam-like model and are valid for straight, slender, homogeneous, isotropic, nonuniform, twisted blades,

undergoing moderate displacement. The equations' system may be coupled with several models for the prediction of the aerodynamic loads. In the present calculations the kinematics of the blade is included through a simplified model in which the blade deformations vary linearly along the radial direction, with the tip flap, lead-lag and torsion deflections coinciding with those measured in the wind tunnel tests.

Finally for the aeromechanical calculations CT4 uses a commercial code, FlightLab™, [23], capable to obtain blade loads, geometrical states and wake inflow for the azimuthally range of interest.

### 3.2 Wake and aerodynamics

The aerodynamics prediction modules of the tools studied herein are quite similar as was the case for the aeroelasticity part. It is evident from Table 1 that all the aerodynamic prediction modules are based on the Boundary Element Method (BEM). This prediction method is used widely in helicopter analysis because of its capacity to model the complex geometry and motions of the vehicle. Other approaches such as the Finite Volume Method (FVM) would require first of all the generation of a domain grid, whereas the BEM methods are based only on boundary surfaces grids, and second the computational resources and convergence time for the FVM would be much greater in comparison to those required by the BEM.

In particular CT1 utilizes an unsteady 3D panel method that allows it to predict the flow field around complex multi-component configurations in arbitrary motion. The methodology is based on the solution of Dirichlet problem for Laplace's equation written for a discrete singularities' distribution simulating the bodies' surfaces. Tangency of the fluid flow to solid boundaries is adopted at every time step following Morino's formulation and the mutual interactions of bodies and wakes are taken into account. The wake simulation can be both prescribed and free. Lifting surfaces generate at every time step a new wake panel row satisfying the Kutta condition. The same code is also used in CT5 for the aerodynamic predictions.

In the corresponding module for the CT2 code, the blade aerodynamics is determined using a lifting line approximation and the wake is represented by filaments forming a vortex lattice. In this case is also used a free wake analysis to compute the wake geometry but with different blade and wake representations with respect to the previous CT. After the free wake geometry is obtained, CT2 models the vortex sheet roll-up. This model is used because, in reality, the blades interact with concentrated vortices and not with a vortex lattice. The CT2 panel method is based on 2D by slices calculation, singularity method, adopting a cloud vortex model option for close BVI prediction.

The aerodynamic module of CT3 is based on a boundary integral formulation for the velocity potential that is suited for helicopter configurations where wake/blade interactions (BVI) occurs, [19]-[21]. This formulation is fully 3D, can be applied to bodies with arbitrary shape and motion, and allows the calculation of both wake distortion and blade pressure field. For a realistic modeling of a close interaction between the wake and a body, a non-zero thickness wake is essential because of the fundamental role played by the vorticity spatial distribution in determining the local fluid flow around the impact region. In order to overcome the above problem, in CT3 the contribution of the wake portion experiencing BVI is expressed in terms of thick vortex distributions(*i.e.* Rankine vortices) rather than in terms of doublets distributions. The shape of the wake can be prescribed or free, *i.e.* part of the solution obtained by a time marching integration scheme in which the wake is moved accordingly to the velocity field computed from the potential solution.

The CT4 uses a full potential code coupled with a 2D laminar/turbulent boundary layer model that allows more physical realism in presence of attached-separated flows up to incipient separation and for flows with strong shocks, [22]. A free wake is used to capture the rotor wake motion and thus model the BVI phenomena. Finally a surface transpiration model is used to account for both blade rigid motions and deformations.

### 3.2.1 Interaction aerodynamics

In presence of strong BVI phenomena, the pressure field along the blade will contain strong fluctuations caused by these interactions. It is necessary thus to insert in the computational codes a module to compute the blade pressure fluctuations caused by BVI events. In the tools presented here this is certainly implemented but detail on how this has been done has been provided only by team 2. In their CT2 code, the BVI pressure fluctuations along the blade are captured by performing a multiple 2D computation of the blade-vortex interaction based on a singularity method. For each section, the BVI events are resolved with a time step as small as  $0.2^\circ$  in order to capture these very impulsive phenomena.

## 3.3 Aeroacoustics

Section 2 already discussed the theory and the equations that could be used for the prediction of rotorcraft noise. In this section will briefly present each aeroacoustic code used in this study. All noise prediction modules in this study are based on the FW-H equation in one of the two integral representations Farassat formulation 1 or formulation 1A, in Equations ( 12 ) and ( 13 ).

In particular, CT1 has an aeroacoustic module that exploits a BEM to determine sound radiation in the linear aeroacoustic field and it has various acoustic formulations, with the option to use Kirchhoff equation or FW-H equation. Several approaches can be adopted for the numerical algorithms: integration of aerodynamic pressures over acoustic surfaces (permeable FW-H), or physical surfaces, with the possibility to choose between Farassat formulation 1 or 1A. In the present calculations CT1 uses Farassat formulation 1A, Equation ( 13 ).

For loading noise computation, CT2 uses its own integral formulation of FW-H equation. This formulation was designed to handle more easily wind tunnel configuration by introducing a term which explicitly takes into account the wind tunnel air speed. The corresponding algorithm computes the integral with a source time approach thought to be less computationally intensive than an algorithm based on retarded time. Actually the retarded time equation does not have to be solved for each blade surface element and for all reception times. Since for a given blade section the BVI aerodynamics prediction code provides the pressure coefficients  $C_p$  on each point discretizing the profile, it is not necessary to use a simplifying compact chordwise approximation.

Regarding code CT3, it implements directly formulation 1A i.e. Equation ( 13 ), without any changes. Some modifications in this formulation are adopted instead in code CT4 that uses formulation 1A extended in order to fully handle the quadrupole term, first term of r.h.s. in Equation ( 11 ), as described in [24].

The remaining code, CT5, implements the Farassat formulation 1, Equation ( 12 ), though using an advanced time algorithm, [25]. This algorithm doesn't require the solution of the transcendent equation for retarded time and thus making it possible to fully couple the noise prediction code to a CFD code, i.e. the aeroacoustic simulation can be run in parallel with the CFD code, [26].

## 4 EXPERIMENTS DESCRIPTION

Within the framework of a previous European cooperative research program on rotorcraft aerodynamics and acoustics (HELISHAPE), a parametric model rotor test was conducted in the open test section of the DNW. These tests used the MWM test rig of DLR and a highly instrumented model of a fully articulated ECF rotor equipped with blades of advanced design and two exchangeable blade tips. One set of blade tips had a rectangular shape whilst the other one had a swept-back parabolic /anhedral shape. The objectives of those experimental tests were to evaluate noise reduction techniques and to validate the partners' aerodynamic and aeroacoustic codes. The aeroelastic blade deflections, especially the torsional and flap-wise deflections that represent important parameters affecting BVI noise and vibrations, were determined from the measured data by means of elementary beam bending theory. In addition, valuable information on the tip-vortex geometry and blade-vortex miss distance was obtained by means of the LLS flow visualization technique.

A comprehensive set of simultaneous acoustic and aerodynamic blade surface pressure data, as well as blade dynamic and performance data were measured during the HELISHAPE tests.

Test Case No.	Rotor Type	Aerodynamic Conditions
TC08.4	7A	Low-speed 6°-descent $\mu = 0.16616$ $C_T/\sigma = 0.08155$ $M_{\omega R} = 0.61651$ $\alpha_{TPP} = 4.50^\circ$ $\theta_{.70} = 2.90^\circ$ $\theta_{1c} = 2.76^\circ$ $\theta_{1s} = -1.42^\circ$
TC09.5	7AD1	Low-speed 6°-descent $\mu = 0.16599$ $C_T/\sigma = 0.08147$ $M_{\omega R} = 0.61816$ $\alpha_{TPP} = 4.22^\circ$ $\theta_{.70} = 3.01^\circ$ $\theta_{1c} = 2.99^\circ$ $\theta_{1s} = -1.69^\circ$

Table 2, flow conditions, [2].

For each acoustic measurement point, the ensemble averaged sound pressure time histories as well as the averaged narrow band power spectra (via FFT) have been calculated. A time domain window was not applied to these data. The conditional sampling approach employed minimized leakage of acoustic energy at the blade passage frequency (bpf) and its harmonics, and thus a time domain window was not required to improve the spectral estimates at these frequencies. The data were further evaluated in terms of A-weighted summary levels.

The two test cases chosen for the assessment of the computational tools discussed above are presented in Table 2. Both of them are low speed  $6^\circ$  descent, a condition in which the wake coming from one blade impinge directly on the following blade generating strong BVI events and thus fluctuations in the blades' loading. This unsteady pressure distribution is the cause of most of the noise produced by the rotor in subsonic flight.

## 5 RESULTS AND CONCLUSION

In this section we will illustrate the validation effort of BVI noise prediction tools conducted within Friendcopter project. The acoustic predictions from the different aeroacoustic codes will be compared to selective HELISHAPE experimental data.

Aerodynamic predictions of the pressure time histories along the leading edge (L.E.), and of the normal force coefficient,  $C_n$ , are presented in Figure 2 - Figure 7. It is clear from the plots that the aerodynamic codes are capable of capturing very closely the test data (shown in black in all the figures). Of particular interest are the zones around the  $90^\circ$  and the  $270^\circ$  degrees of azimuth where all the BVI encounters occur. The codes predict the trends of the pressure fluctuations quite well, with small differences seen in the magnitude of the pressure signal compared to the experiments - except perhaps for the most extreme pressure peaks. Considering that the spanwise positions presented,  $r/R=0.92$  and  $r/R=0.98$ , are those in which the BVI are most accentuated, the predictions from codes CT1 CT2 CT3 CT5 can be considered to be in very good agreement with the test data. Examination of the  $C_n$  plots for the same spanwise sections as the pressure time histories, shown in Figure 6 and Figure 7, again indicate that all codes, except for CT4 whose  $C_n$  prediction differs most from the measured loads, captured the characteristics of the blade aerodynamics very satisfactorily.

Once assured from the above results that the aerodynamics, and thus the dynamics of the rotor, have been well modeled, it is possible to move on to the analysis of the aeroacoustic results. The noise footprints will be presented in OASPL and not A-weighted [dBa] since the input required by HELENA, the optimization software produced within Friendcopter, is not weighted thus it is more meaningful to compare the results not weighted.

Comparisons between the results from the aeroacoustic code CT1 and the WT tests, see Figure 8 and Figure 9, show that the noise directivity pattern is well predicted for both test cases considered and that the amplitude of sound radiation is predicted quite well, with differences of less than 0.5 [dB] at the highest values throughout the whole simulated field. The BVI interactions, typical of the advancing region, are thus reproduced well. The peak-to-peak excursions in the retreating blade side, however, are not predicted very well with the theoretical results being lower in magnitude to the experimental data. This is thought to be due to the CT1 code not fully capturing the complex flow phenomena taking place over this rotor azimuthal sector.

Referring to the results from the CT2 aeroacoustic code, it can be seen in Figure 10 and Figure 11 that the comparison of the maximum noise levels between the predicted and the experimental results is relatively good, with any differences lying within a 2.0dB band. The directivity prediction for the simulated results appears to be shifted slightly upwards and to be too narrow. The retreating side directivity as well as the corresponding noise levels are correctly captured.

Results from the third aeroacoustic code CT3, show that the predicted noise footprints are in good agreement with the measured levels, both in amplitude and in directivity values, see Figure 12 and Figure 13. The difference between the maximum values is within a 2 dB range. The directivity patterns on the advancing side are in very good agreement whilst a slight underestimation is present in the retreating side, more accentuated in the TC09.5 case.

The results from the CT4 aeroacoustic code appear to show very poor correlation with respect to the experimental data and are not included. This is of course not very surprising given the fact that this code gives very poor Cn correlations with test data (see Figure 6 and Figure 7). The reasons for this are not presently known. It has been verified that time-step, observation time, blade motion/deformation are adequate and also the effect of redundant wake parts are not significant. It is thus postulated that the poor correlation might be due to the fact that the current wake inflow model used in CT4 is probably inadequate to properly capture the complex flow present in these test cases.

The results from the CT5 aeroacoustic code are in good agreement with the WT test results. The results show a slight underestimation of about 2 dB in amplitude but the directivity patterns are well predicted in the advancing side, see Figure 14 and Figure 15.

Having established an overall view of the capability of the different methods to predict BVI noise, it will be of interest to examine in more detail the acoustic pressure time histories on the microphones. Actually this examination enable us to assess if the physics of BVI (number of peaks, magnitude and position of the dominant peak) are well captured by the both the aerodynamic and the aeroacoustic computations.

Examination of the acoustic pressure time histories, see Figure 16, shows that all the codes to a greater or lesser effect have been able to capture the physics of the BVI phenomena, with best agreement been shown by the CT3 and CT1 codes.

For the CT2 code, in the previous analysis, a directivity shift was observed with respect to experiment because of an azimuthal shift in predicted BVI occurrences. Thus the computed acoustic signal and the measured one could not be compared at the same location (X,Y) because one would have compared acoustic signals corresponding to different physical phenomena. In order to consider the same physical events, Figure 17 compares the computed acoustic signal at the predicted maximum BVI noise location to the measured signal at the experimental maximum BVI location represented by the black squares in Figure 10. The maximum BVI locations were determined by an analysis of the dBA noise footprints in order to eliminate low frequency loading noise. This analysis is not presented here for concision reasons. As it can be seen in Figure 17, CT2 seems to capture well the physics of the BVI events: the number of peaks and their corresponding amplitude.

In conclusion, the results obtained from the computational tools presented herein confirm their capabilities to provide aeroacoustic predictions that are in good agreement with the experimental data for the test cases chosen. The majority of codes are able to capture well the physics of the acoustic phenomena on the advancing side but show limitations along the retreating side of the blade mainly due to the difficulties of capturing properly the complex flow phenomena associated with blade-vortex interaction along this sector. Overall, some quantitative differences are evident from the comparisons discussed above. These studies have been useful in highlighting them and thus give the researchers the opportunity to better understand

the shortcomings of each aeroacoustic code and the modifications required to improve its performance.

Given the satisfactory results obtained so far by most of the aeroacoustic codes on the test cases examined, it is planned in the near future to extend their application to full scale helicopters in a simulated operational environment. This will be done in order to establish optimum flight envelopes/trajectories that could be used to assist the Friendcopter consortium in their aim towards the design of more environmentally friendly, from the noise point of view, helicopters.

## 6 ACKNOWLEDGMENTS

This work is supported by the European Union under the 6th Framework Programme for Research and Technological Development, Friendcopter project. Also thanks must be given to the HELISHAPE consortium members for making available the experimental data used.

## 7 REFERENCES

- [1] Friendcopter Proposal, Integrated Project Proposal Part B.
- [2] Hounjet, M.H.L, "Common Test Cases for Task 2.2.2", Friendcopter report.
- [3] Algermissen, G., Wagner, S., "Computation of helicopter BVI noise by coupling free-wake, Euler and Kirchhoff method", AIAA/CEAS Aeroacoustics Conference, 4th (19th AIAA Aeroacoustics Conference), Toulouse, France, Collection of Technical Papers. Pt. 1; UNITED STATES; 2-4 June 1998. pp. 217-225. 1998
- [4] Visingardi, A., D'Alascio, A., Pagano, A., Renzoni, P., "Validation of CIRA's Rotorcraft Aerodynamic Modelling System with DNW experimental data", European Rotorcraft Forum, 22nd, Brighton, United Kingdom, Proceedings. Vol. 1; UNITED KINGDOM; 17-19 Sept. 1996. pp. 57.1-57.14. 1996
- [5] Rouzaud, O., Raddatz, J., Boniface, J. C., "Euler calculations of multibladed rotors in hover by DLR and ONERA methods and comparison with HELISHAPE tests", AHS, Annual Forum, 53rd, Virginia Beach, VA; UNITED STATES; 29 Apr.-1 May 1997. pp. 1102-1114. 1997
- [6] Schultz, K.-J., Splettstoesser, W. et al., "A Parametric Wind Tunnel Test on Rotorcraft Aerodynamics and Aeroacoustics (HELISHAPE) - Test Documentation and Representative Results", 22nd European Rotorcraft Forum, Brighton, U.K., 1996.
- [7] Lighthill, M. J. "On sound generated aerodynamically.I. general theory." Proceedings of the Royal Society of London, Series A, Mathematical and Physical Sciences 211, 1107 (1952), 564-587.
- [8] Ffowcs Williams, J. E., and Hawkings, D. L. "Sound generation by turbulence and surfaces in arbitrary motion". Philosophical Transactions of the Royal Society of London. Series A, Mathematical and Physical Sciences 264, 1151 (1969), 321-342.
- [9] Goldstein, M.E., "Aeroacoustics", New York, McGraw-Hill International Book Co., 1976.
- [10] Farassat, F., "Linear Acoustic Formulas for Calculation of Rotating Blade Noise," *AIAA Journal*, Vol. 19, No. 9, 1981, pp. 1122-1130
- [11] Farassat, F. "Introduction to generalized function with applications in aerodynamics and aeroacoustics." Tech. rep., NASA Technical Paper 3428, 1996.
- [12] di Francescantonio, P., "A New Kirchhoff Formulation for Transonic Rotor Noise," 22<sup>nd</sup> European Rotorcraft Forum, Brighton, UK, September 1996.

- [13] Schmitz, F.H., "Rotor Noise", Aeroacoustics of Flight Vehicles: Theory and Practice, Vol.1, Ch. 2, NASA TR 90-3052, 1991
- [14] Ponza, R., "Flying Helicopters Acoustic impact assessment: towards a more realistic simulation methodology", ECCOMAS 2004
- [15] P. Beaumier and P. Spiegel, "Validation of ONERA Aeroacoustic Prediction Methods for Blade-Vortex Interaction Noise by HART Test Results," 51st Annual Forum of the American Helicopter Society, Ft Worth, TX, May 1995.
- [16] G. Rahier, and Y. Delrieux, "Improvement of Helicopter Rotor Blade-Vortex Interaction Noise Prediction Using a Rotor Wake Roll-up Model," 1st Joint CEAS/AIAA Aeroacoustics Conference (16th AIAA Aeroacoustics Conference), Munich, June 1995.
- [17] Hodges, D.H., and Dowell, E.H., 'Nonlinear Equation for the Elastic Bending and Torsion of Twisted nonuniform Rotor Blades,' NASA TN D-7818, 1974.
- [18] Hodges, D.H., and Ormiston R.A., 'Stability of Elastic Bending and Torsion of Uniform Cantilever Rotor Blades in Hover with Variable Structural Coupling,' NASA TN D-8192, 1976.
- [19] Gennaretti, M., and Bernardini, G., "A Novel Potential-Flow Boundary Integral Formulation for Helicopter Rotors in BVI Conditions," AIAA Paper 2005-2924, Proceedings of the 11th AIAA/CEAS Aeroacoustics Conference, Monterey, California, May 2005
- [20] Morino, L., "A General Theory of Unsteady Compressible Potential Aerodynamics," NASA CR-2464, 1974
- [21] Bernardini, G., Ianniello, S., Gennaretti, M., "Analysis of Blade Deformation Effect on Rotor BVI Noise Prediction," 31st European Rotocraft Forum, Firenze, Italia, 13-15 September 200.
- [22] A. Pagano, M.H.L. Hounjet, J.V. Miller, M. Gracey, and A Pisoni. ROSAA: A European Simulation System for the Multidisciplinary Numerical Prediction of Rotor Phenomena. In Proceedings of ECCOMAS 2000, Barcelona, Sept 2000
- [23] Advanced Rotocraft Technology, Mountain View, Flightlab™
- [24] Ianniello, S., Quadrupole Noise Predictions Through the Ffowcs Williams-Hawkings Equation, AIAA Journal, Vol. 37, N. 9, pg. 1048-1054, September, 1999.
- [25] Prieur, J. ,"Aeroacoustic Integral Methods, Formulation and Efficient Numerical Implementation", Aerospace Science Technology, Vol.5 ,2001, pp. 457-468
- [26] Casalino, D., "An advanced time approach for acoustic analogy predictions", *Journal of Sound and Vibration*, 261, 2003, 583-612

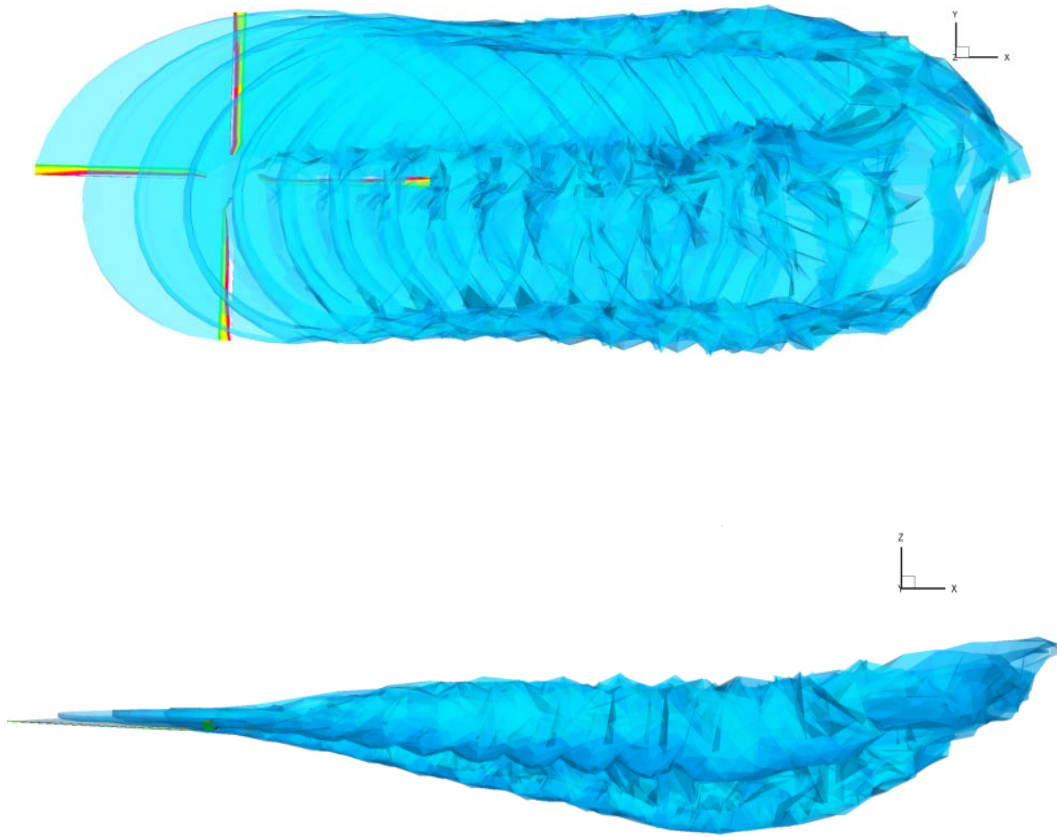


Figure 1: BVI visualization, detail of wake/blade interactions. Upper and side views, CT1

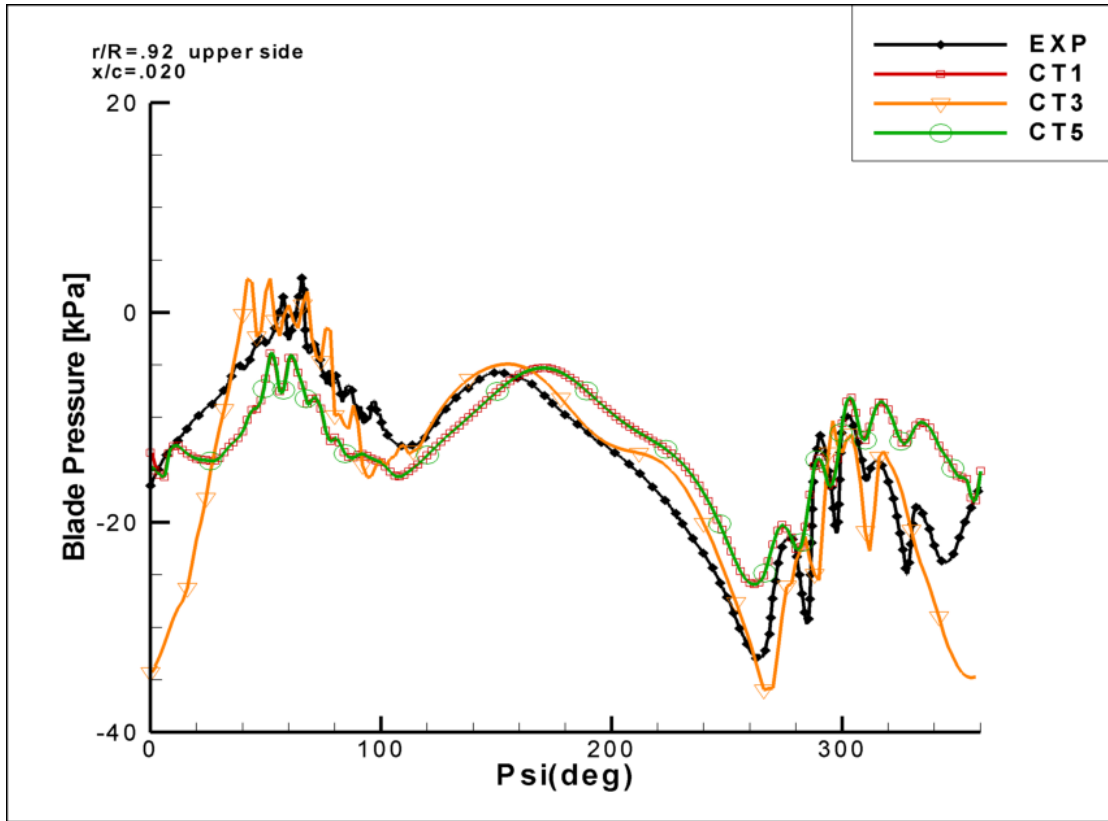


Figure 2: Pressure time history, upper surface,  $x/c=0.02$ ,  $r/R=0.92$ , TC08.4

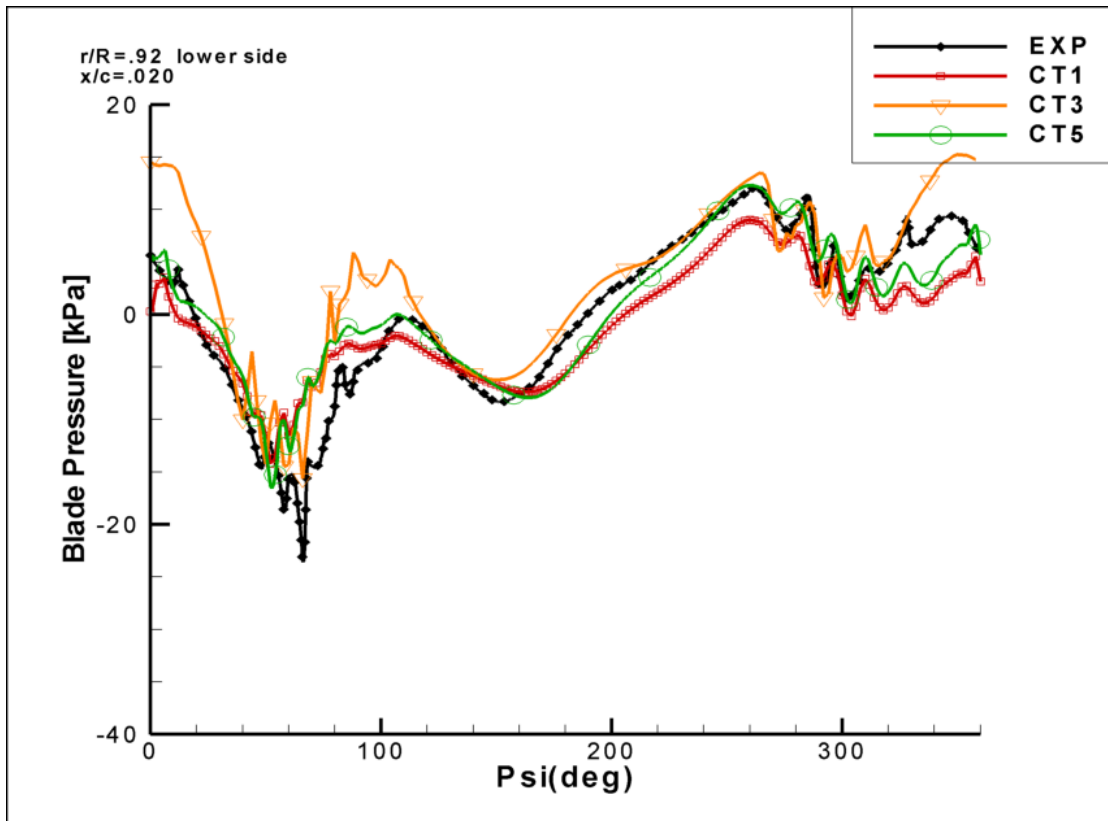


Figure 3: Pressure time history, lower surface,  $x/c=0.02$ ,  $r/R=0.92$ , TC08.4

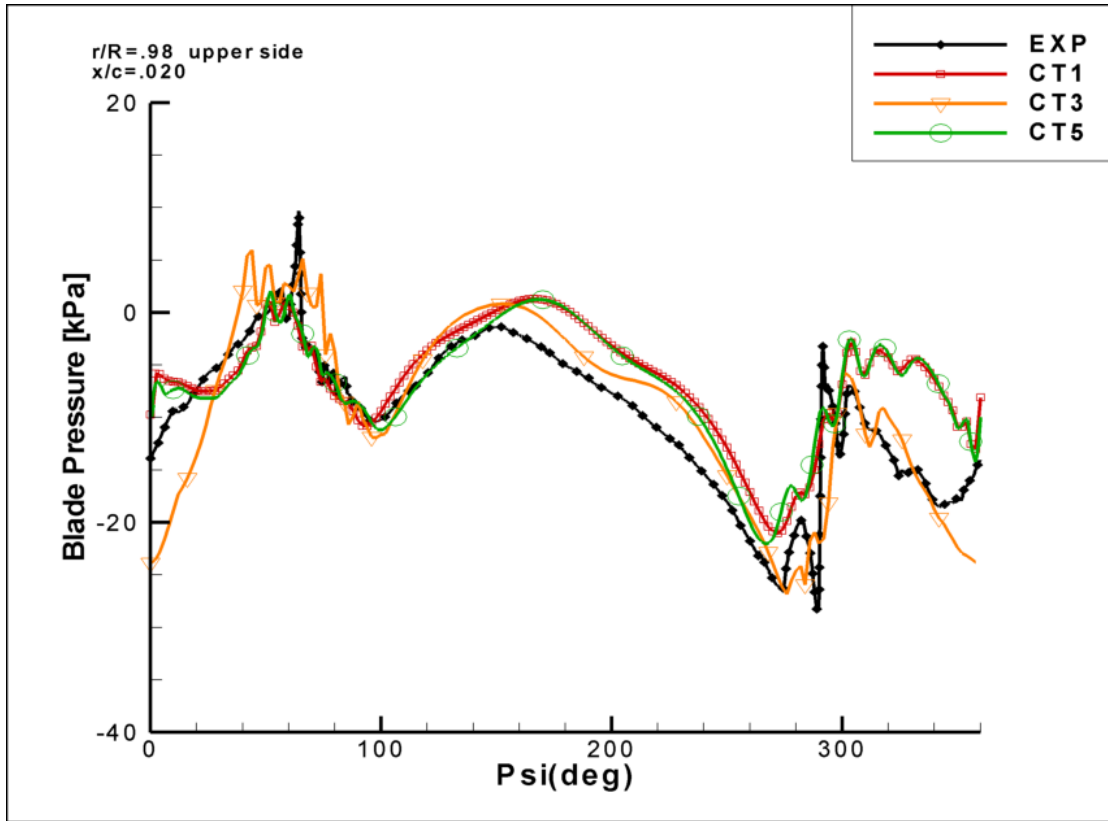


Figure 4: Pressure time history, upper surface,  $x/c=0.02$ ,  $r/R=0.98$ , TC09.5

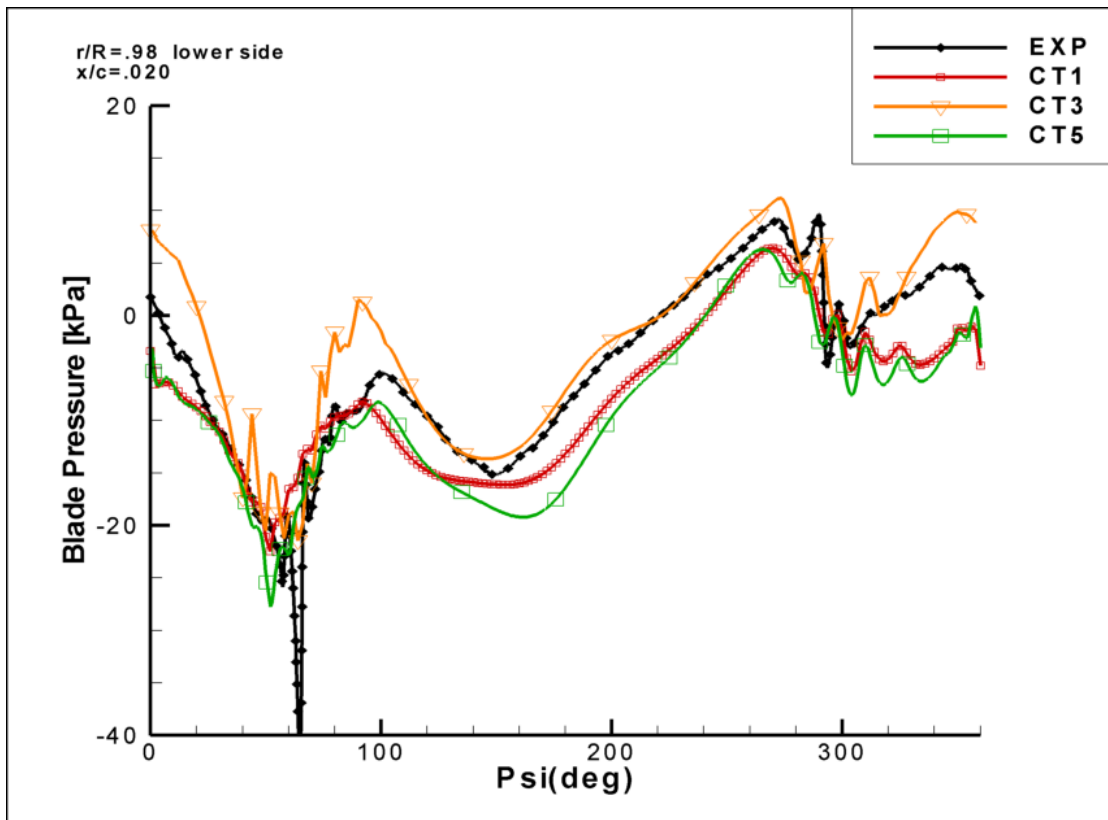


Figure 5: Pressure time history, upper surface,  $x/c=0.02$ ,  $r/R=0.98$ , TC09.5

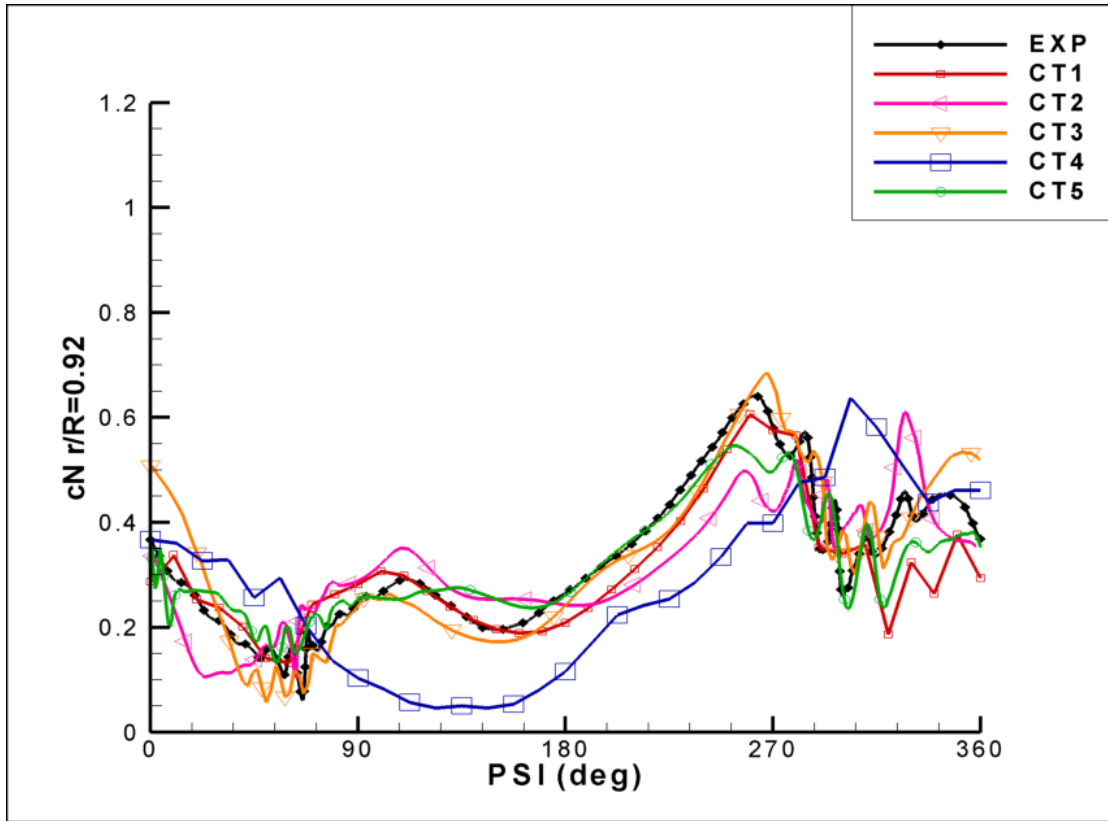


Figure 6: Normal force coefficient time history,  $r/R=0.92$ , TC08.4

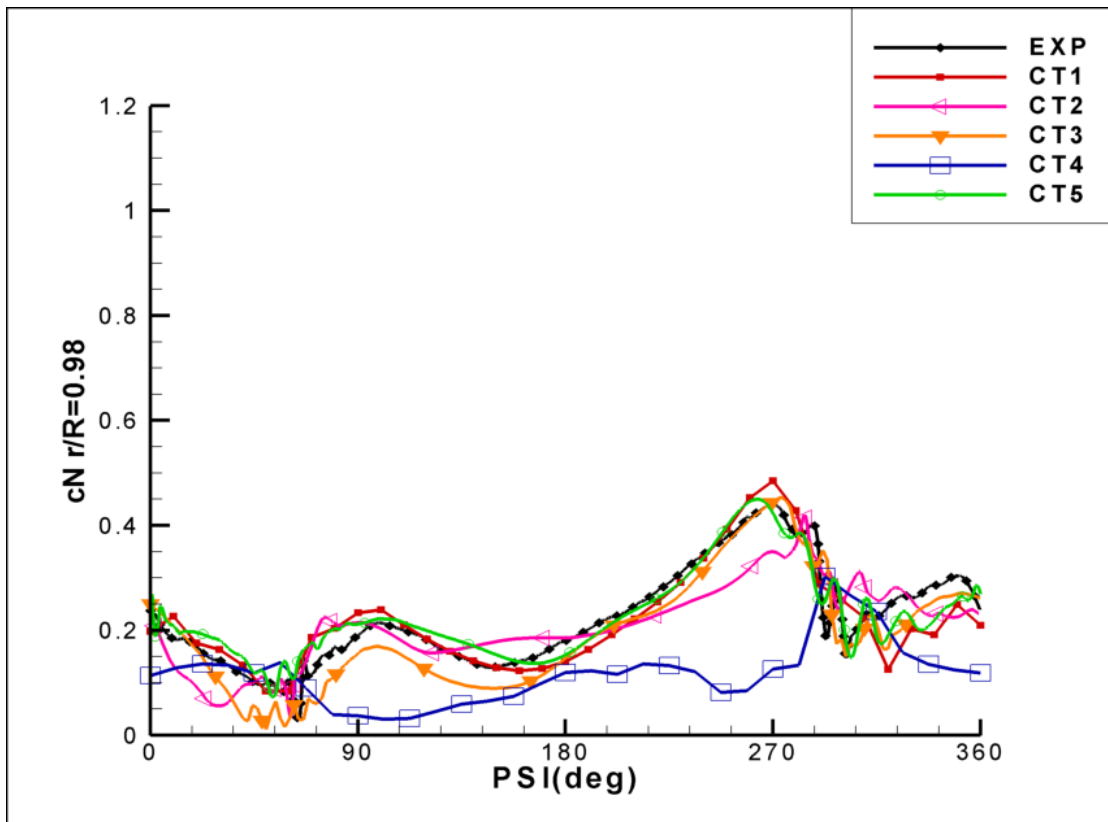
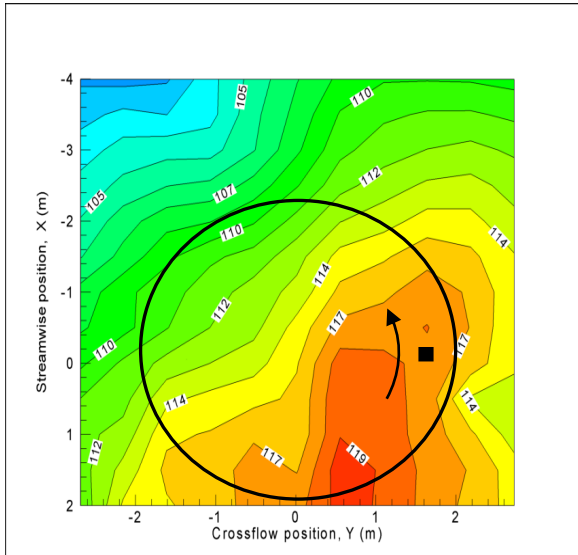
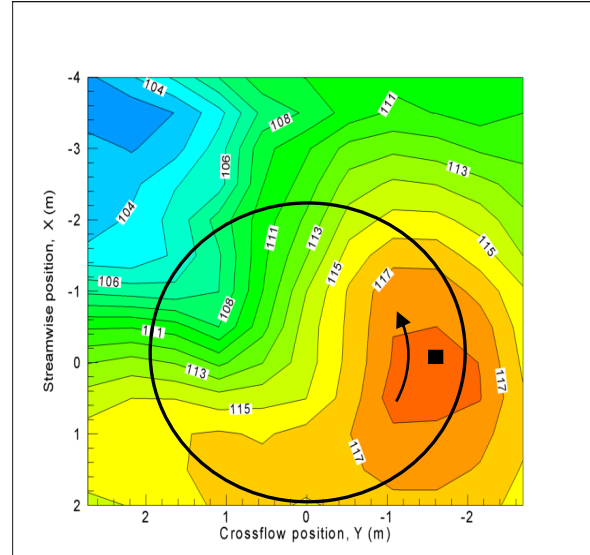


Figure 7: Normal force coefficient time history,  $r/R=0.98$ , TC08.4

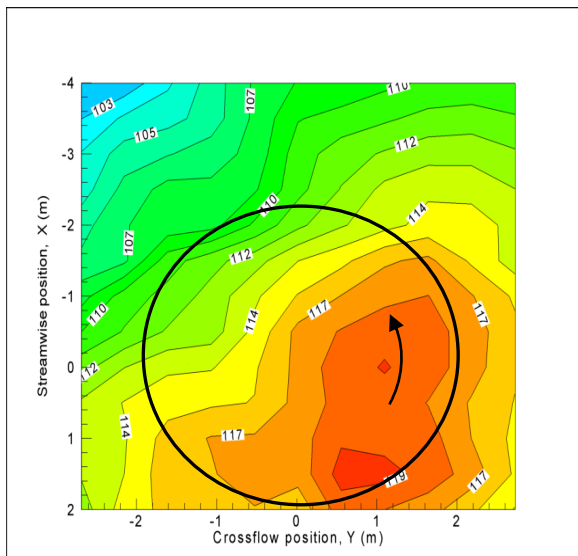


a

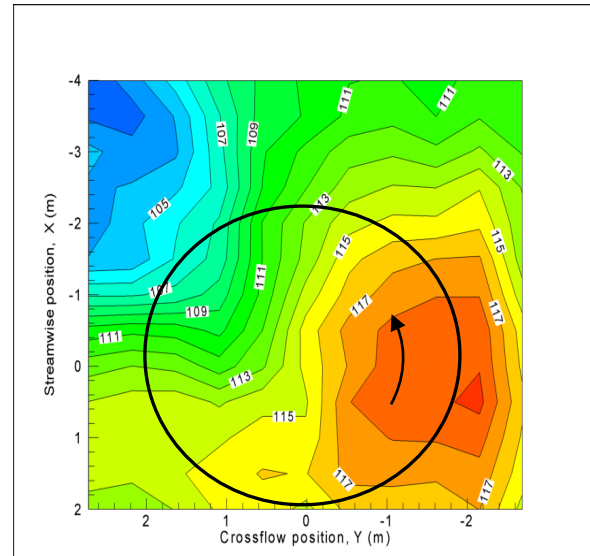


b

Figure 8: Comparison between simulated (a) and experimental (b) noise footprints. CT1, TC08.4

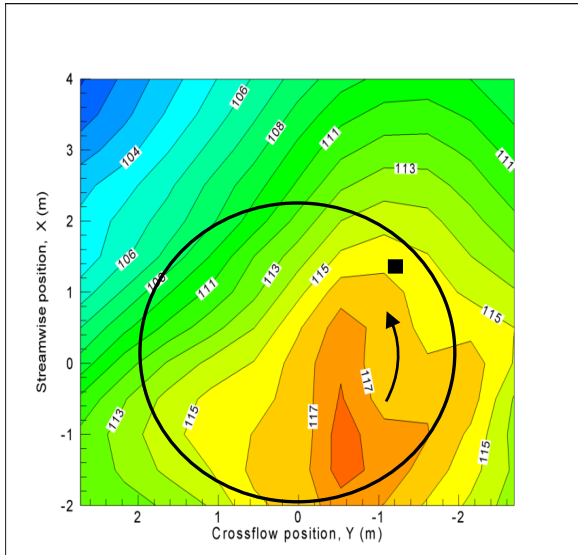


a

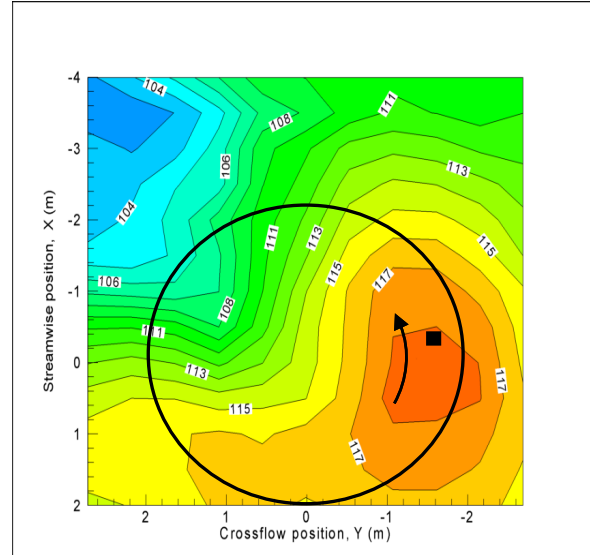


b

Figure 9: Comparison between simulated (a) and experimental (b) noise footprints. CT1, TC09.5

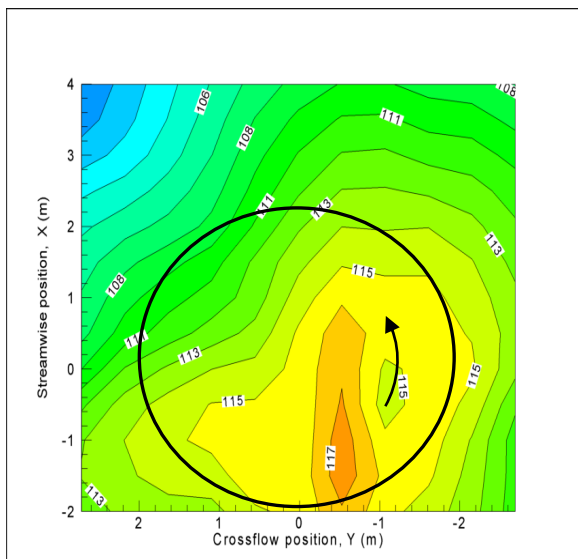


a

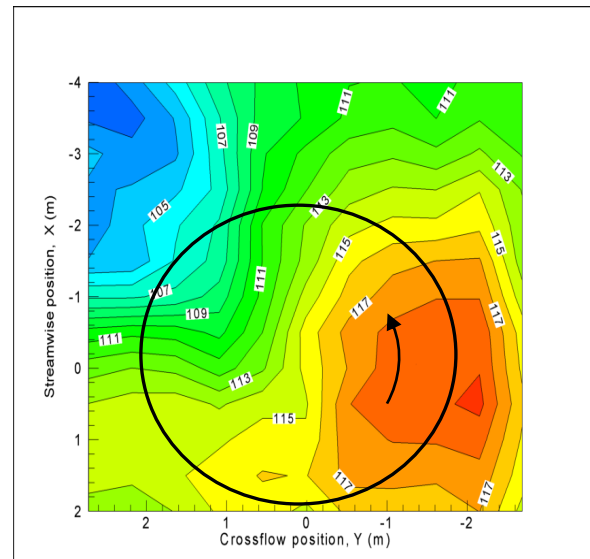


b

Figure 10: Comparison between simulated (a) and experimental (b) noise footprints. CT2, TC08.4. (The black squares represent the maximum dBA locations at which the acoustic signals will be compared)

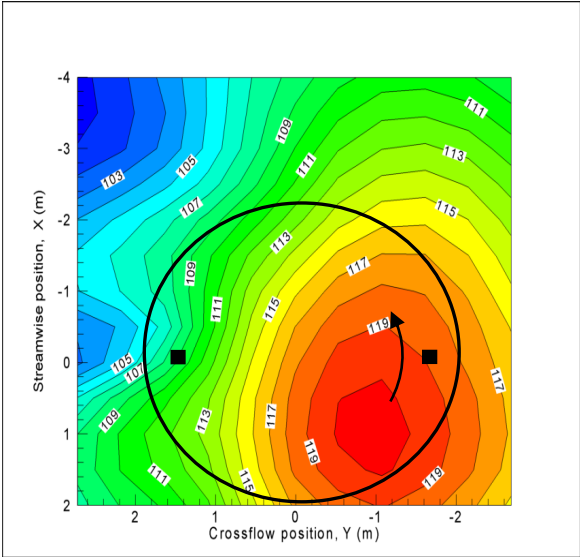


a

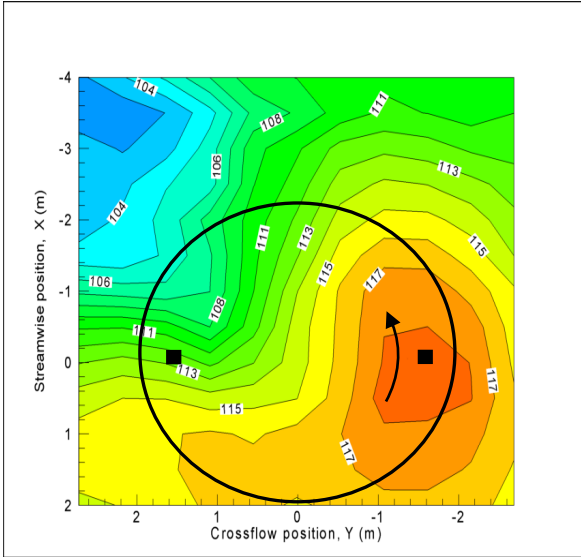


b

Figure 11: Comparison between simulated (a) and experimental (b) noise footprints. CT2, TC09.5

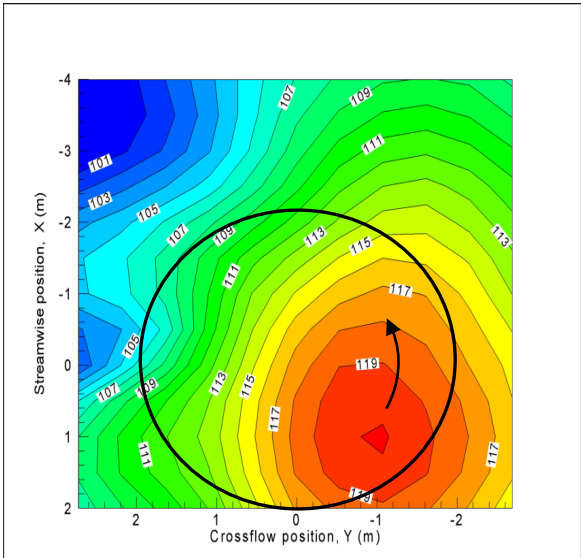


a

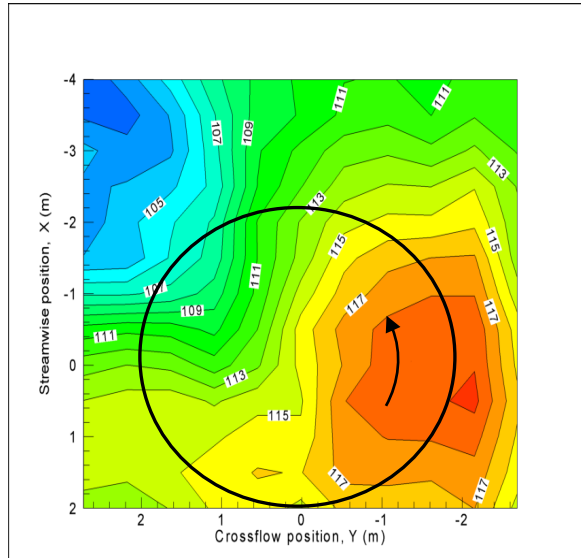


b

Figure 12: Comparison between simulated (a) and experimental (b) noise footprints. CT3, TC08.4

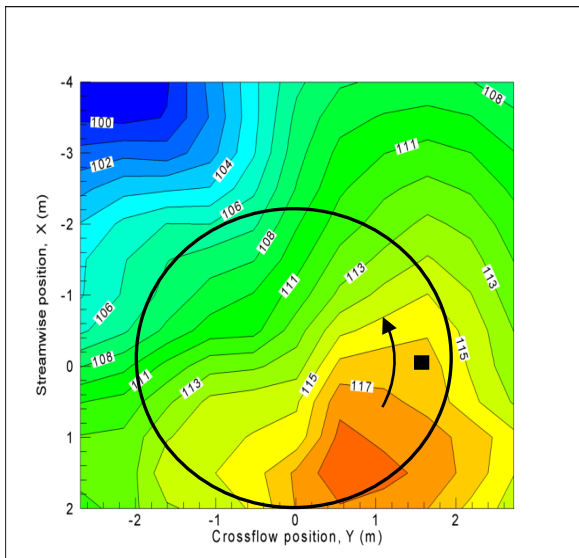


a

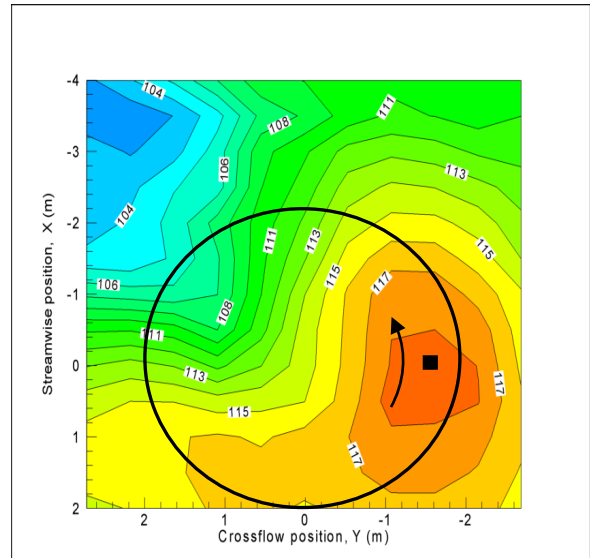


b

Figure 13: Comparison between simulated (a) and experimental (b) noise footprints. CT3, TC09.5

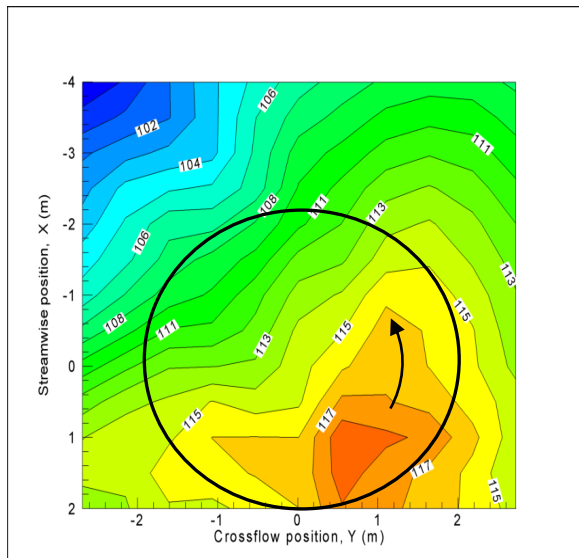


a

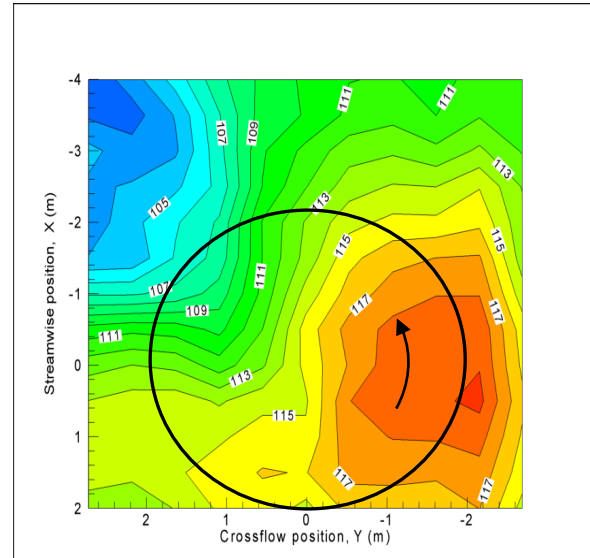


b

Figure 14: Comparison between simulated (a) and experimental (b) noise footprints. CT5, TC08.4

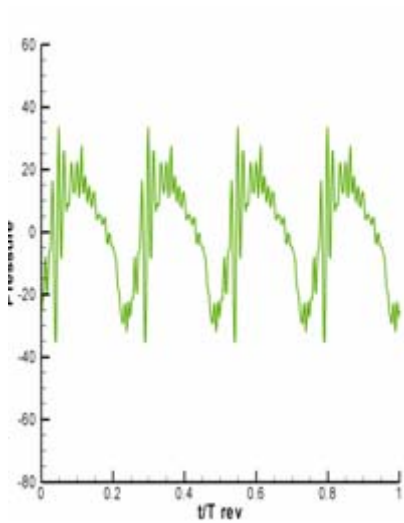
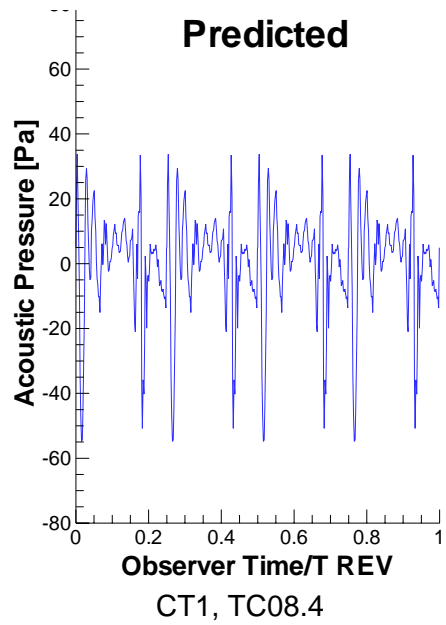
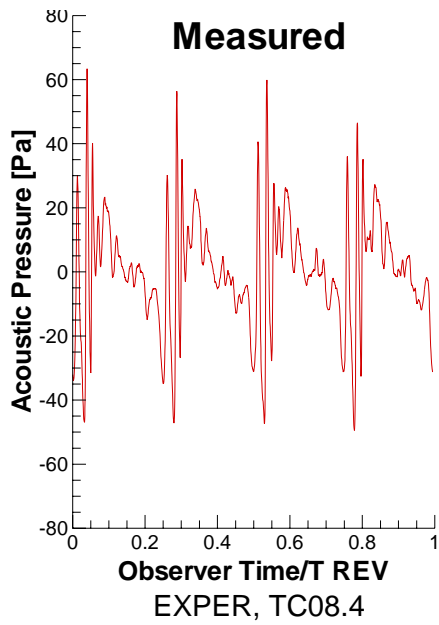


a

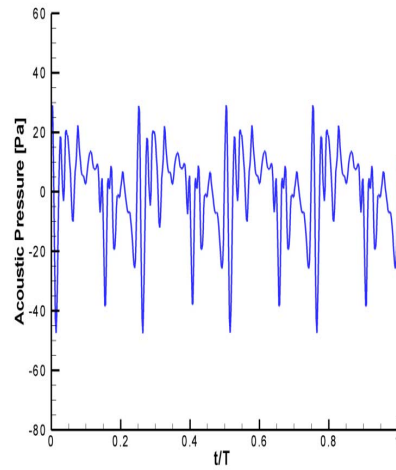


b

Figure 15: Comparison between simulated (a) and experimental (b) noise footprints. CT5, TC09.5



CT3, TC08.4



CT5, TC08.4

Figure 16: Comparison between experimental and predicted pressure time histories, case TC08.4 in Table 1, radiated by 7A, advancing side point, black squares in the footprint figures

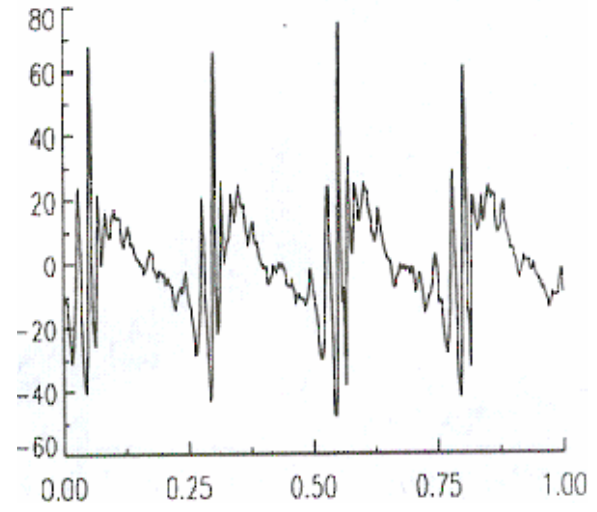
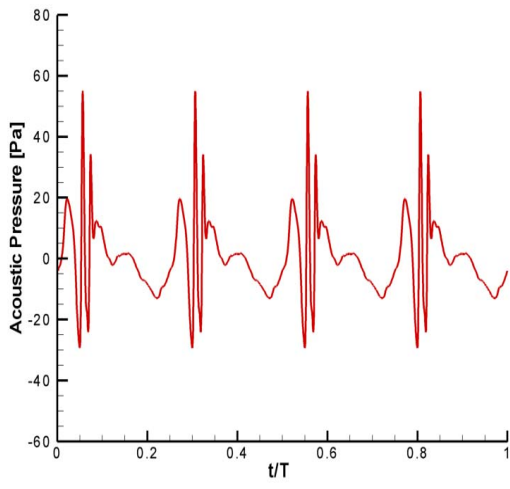


Figure 17: Team CT2. Comparison between predicted and experimental pressure time histories, case TC08.4 in Table 1, radiated by 7A, at the maximum noise locations, Figure 10